Phase-Transition Plasticity Response in Uniaxially Compressed Silicon Nanospheres

P. Valentini,[1] W. W. Gerberich,[2] and T. Dumitrică[1,*]

[1]Department of Mechanical Engineering, Institute of Technology, University of Minnesota, Minneapolis, Minnesota 55455, USA
[2]Department of Chemical Engineering and Materials Science, Institute of Technology, University of Minnesota, Minneapolis, Minnesota 55455, USA

(Received 19 May 2007; published 26 October 2007)

We present a microscopic description for the response of crystalline Si nanospheres up to 10 nm in radius for various uniaxial compression levels. The behavior at low compressions closely resembles the Hertzian predictions. At higher compressions the creation of a new β-tin phase in the particle core leads to (i) volumetric changes (ii) an increase in elastic moduli, and (iii) significant hardening. Further, (iv) a reversible character of the transformation is obtained with molecular dynamics simulations. The agreement of (i)–(iv) with recent experimental findings challenges the current exclusive view of a dislocation plasticity response in somewhat larger nanoparticles. The phase-transition path should dominate in ultrasmall structures, where dislocation activity is prohibited.

DOI: 10.1103/PhysRevLett.99.175701 PACS numbers: 64.70.Nd, 62.25.+g, 62.50.+p, 82.20.Wt

Understanding nanoscale plasticity of Si is of both fundamental importance and of practical interest for nanotechnological innovation [1]. While dislocation plasticity and phase transitions have been widely documented in the nanoindentation of crystalline bulk [2–4], the response of the nanoscale is subject to dispute. Using a nanoindenter, compression tests were performed recently [5] on a sparse population of defect-free Si nanoparticles 20 to 100 nm in radius. Notably, hardness values in the 20–50 GPa range were measured, exceeding the 12 GPa of bulk Si. The underlying hardening mechanism was not directly observed. The proposed model [5] was solely based on the nucleation of dislocations. However, it is accepted that dislocations cannot nucleate below a critical size. Thus, to rationalize the behavior of the smallest scale and the transition to the dislocation dominated scale, it is important to identify other response mechanisms.

Here we investigate such an alternative mechanism involving a cubic-diamond $\rightarrow$ β-tin phase transformation. This type of response was observed before in the nanoindentation of bulk Si [3,4] and in the hydrostatic compression of Si crystallites [6]. Moreover, a recent molecular dynamics (MD) study [7] on the low-energy impact of Si nanospheres detected an ephemeral β-tin phase in the particle instead of the expected dislocation activity. Thus, we inquire whether the β-tin phase can be accommodated in uniaxially compressed Si nanoparticles and what would be the observable consequences. Our simulations indicated that this new phase nucleates in the center of the particle and grows under higher loads. Remarkably, several important features obtained in the experimentation [5] are reproduced: The severely compressed particles have a smaller volume, a higher elastic modulus, and are harder. Upon unloading, a reverse transformation was obtained.

The interaction of Si cores is described here with the bond-order potential of Tersoff [8] as incorporated in the package Trocadero [9]. This potential correctly predicts the pressure-induced transformation from cubic to β-tin [7]. The isotropic compression of very small Si nanoparticles has been studied previously with tight-binding [10] and density functional theory (DFT) [11]. The advantage of the present classical treatment is that it allows for efficient simulations of rather substantial systems. Here we deal with three spherical Si particles of radii $r_{01} = 2.5$ nm, $r_{02} = 5$ nm, and $r_{03} = 10$ nm, containing 3,870, 31,075, and 209 461 atoms, respectively. Notably, unlike in previous studies [10,11] we are applying uniaxial strain by incorporating in the simulations two platens, each containing 3200 frozen atoms.

In preparation for the simulations, the particles have been carved out of the bulk and structurally relaxed. Table I reports their cohesive energies (U_c), showing an expected stability increase with size. Next, each particle was placed between the two platens, as shown in Fig. 1(a). To avoid bonding, a higher repulsion was imposed between the particle-platen atoms. Our simulations are focusing on the nonthermal response and the compression process was simulated by giving a 0.25 Å incremental displacement to the platens towards the particle, followed by structural relaxations. A series of useful indicators was recorded, including the local cohesive energy, the particle-platen contact radius [7] (a), the force on the platen (P), and the averaged contact stress [7] ($\sigma_m = P/\pi a^2$). The procedure

TABLE I. Cohesive energies, stiffnesses, and Young's moduli in the [100] direction for the three spherical nanoparticles used in the compression simulations, and for Si bulk.

System:	$Si_{3,870}$	$Si_{31,075}$	$Si_{209,461}$	Si bulk
r_0 (nm)	2.5	5	10	···
$U_c(eV/\text{atom})$:	4.36	4.50	4.56	4.63
$U''(eV/\text{atom})$:	4.20	4.21	4.78	···
$E_p^0(GPa)$:	85	102	104	140

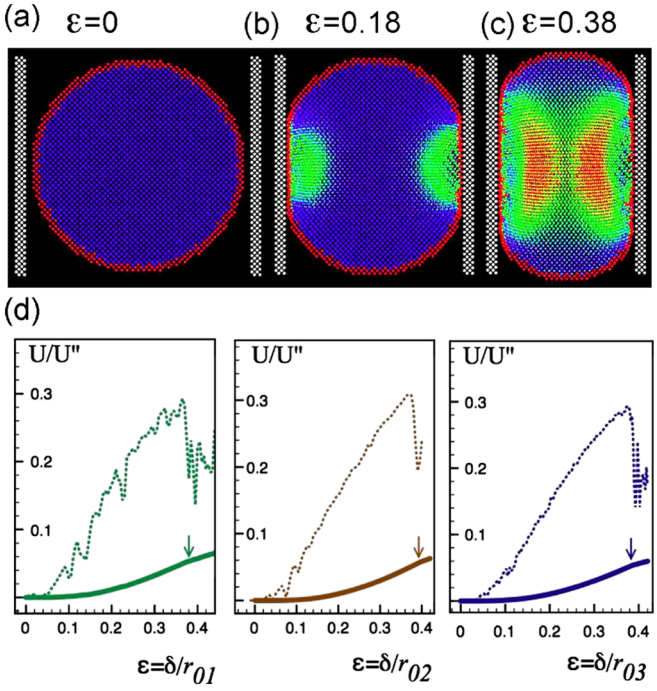

FIG. 1 (color online). (a)–(c) Elastic compression stages of the 5 nm particle. (d) Strain energy versus strain for all three particles. Dotted lines are the derivatives $d(U/U'')/d\varepsilon$, while the down arrows mark the elastic regime limit at $\epsilon \sim 38\%$.

was repeated until a maximum compression point was reached, after which the platens retracted with the same protocol.

We first describe the obtained response to relatively low loads. Figures 1(a)–1(c) depict three successive configurations from the compression of the 5 nm particle. The local potential energy information is carried by a color code of blue (dark gray) at 4.6 eV (U_c for bulk Si), green (light gray) at 4.3 eV (U_c for bulk β-tin), to red (gray) at 3.5 eV. Inspection of the uncompressed particle in Fig. 1(a) reveals that the core atoms have practically the cohesion of the bulk and a significant decrease in binding can be noted only in the 2–3 surface layers. Next, Fig. 1(b) shows a representative instant for the initial stages of the compression. An interesting magnitude associated with local U_c is the local strain. The particle flattens at the contacts, producing a strain increase in the region around the platens. As the indentation progresses the strain field reaches higher values and expands toward the particle's center. Figure 1(c) corresponds to a critical platen displacement (δ) that causes the intersection of the two strain fields. Note that a quasistatic unloading of the configurations shown in Fig. 1(b) and 1(c) practically regains the original shape.

Figure 1(d) plots, for all three particles, the strain energy U as a function of the applied strain $\varepsilon = \delta/r_0$. At small ε the energy grows as $U/U'' = \varepsilon^2/2$, with the U'' stiffness values entered in Table I. While the inflection points in the energy curves are hardly visible, the plot of derivative unambiguously shows an increase in particle compliance at 38%, which marks the limit of the elastic regime.

The noted localized aspect of the deformation makes it interesting to inquire if aspects pertinent to the macroscopic contact theory of nonconforming bodies [12] are applicable. In Fig. 2(a) we plotted a^2 as a function of ε. The Hertzian predictions (dashed lines), obtained with

$$a^2 = \delta r_0 = \varepsilon r_0^2, \tag{1}$$

follow closely the atomistic data, indicating the validity of this theory. It follows [12] that we can connect the applied load to the vertical displacement through the elastic properties of the particle (i.e., Young's modulus E_p^0 and Poisson's ratio $\nu = 0.218$), as

$$P = \frac{4E_p^0\sqrt{r_0}}{3(1-\nu^2)}\delta^{3/2} = \frac{4E_p^0 r_0^2}{3(1-\nu^2)}\varepsilon^{3/2}. \tag{2}$$

In Fig. 2(b) we plotted this dependence based on our atomistic data and used Eq. (2) to calculate E_p^0. The obtained values, entered in the last line of Table I, show a weak size dependence. Further, to illustrate the success of this approach, Fig. 2(b) shows also the prediction made with formula (2) and the E_p^0 values of Table I. Note that the obtained size-effect in the E_p^0 values reflects the high surface-to-volume ratio, which constitutes a "weakness" for the particles. The lower-than-bulk values agree with recent measurements [5] but care should be exercised as experimental data captured the softer SiO_2 outside layer.

The particle hardness, defined as the averaged contact stress at the maximum loading, was next computed. The σ_m-P curves of Fig. 3 show that as the load is increased the pressure on the plates rapidly rises to settle at ~18 GPa. This hardness value compares well with the data obtained in the indentation size-effect studies [13] of the Si surface, ~18.5 GPa at depths below 1 nm, and ~23.3 GPa at depths between 1 and 5 nm.

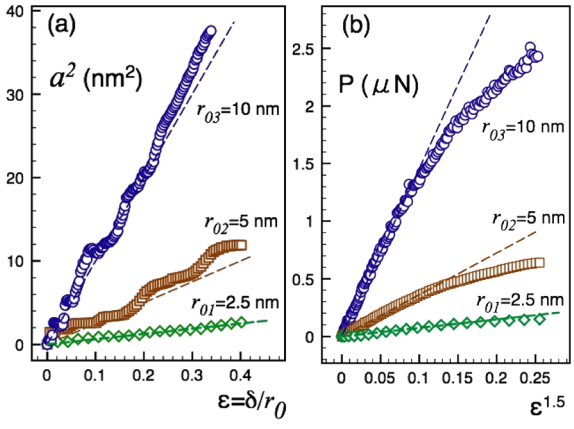

FIG. 2 (color online). (a) The square of contact radii versus the applied strain. (b) Applied force versus the square root of cubic strain. Dashed lines represent the Hertzian predictions.

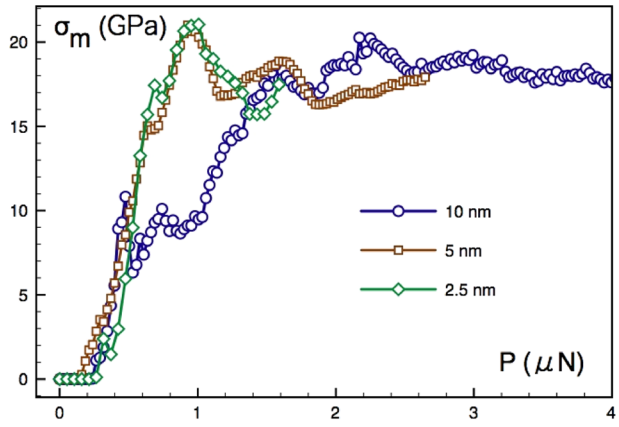

FIG. 3 (color online). The contact stress versus load.

We now discuss the response to higher loads. Figure 4 summarizes the behavior of the 5 nm particle under three loading-unloading cycles, with each cycle achieving larger excursions. In Fig. 4(a), showing the obtained P-δ curves, we note that on the first cycle beyond the critical displacement (marked with an arrow) there is a decrease in slope, followed by a steeper increase up to the maximum loading point. The unloading curve is also significantly steeper than the original elastic one and leads to an unstrained particle with residual deformation. The staircase features, characteristic for dislocations and seen in the nanoindentation of larger particles [5], are not present. For the next two cycles the unloading curves get steeper as the excursions get larger, signaling an increase in particle stiffness. Employing the usual relation [5] $E_p = (1/2a)dP/d(\delta)$, we extracted from the three unloadings Young's moduli of 138, 266, and 585 GPa. The end of the cycle particle volumes, computed with Delaunay triangulation, were 574, 558, and 533 nm^3, respectively. (The original volume was 605 nm^3). In Fig. 4(b) the σ_m-P curves are plotted. Remarkably, the particle exhibits an increase in hardness, up to a ~30 GPa value. This trend is consistent with the repeat load cycles experimental results [5].

What is the microscopic origin of the particle size reduction coupled with the increase in hardness? From Fig. 4(b) we note that due to the small contacts, the resulting high pressures would be able to cause a β-tin phase transition in bulk Si (10–15 GPa [4]). Thus, we examined the structures of the compressed particles and Fig. 4(c) shows cross sections of the 5 nm particle as obtained at the end of the three unloading cycles. A new phase in the core can be noted, with U_c of the β-tin.

Figure 5, showing the radial distribution function $g(r)$ for the last structure of Fig. 4(c), confirms that the newly created phase is β-tin. The first peak at 2.35 Å corresponds to the first neighbor distance in cubic diamond and thus is due to the residual tetrahedral structure. The second and third peaks are correlated with the first and second neighbor distance in bulk β-tin (2.54 Å and 2.57 Å, respectively). The slight discrepancy in location reflects the strain in the particle. The next three peaks fall very well on the neighboring distances of the β-tin.

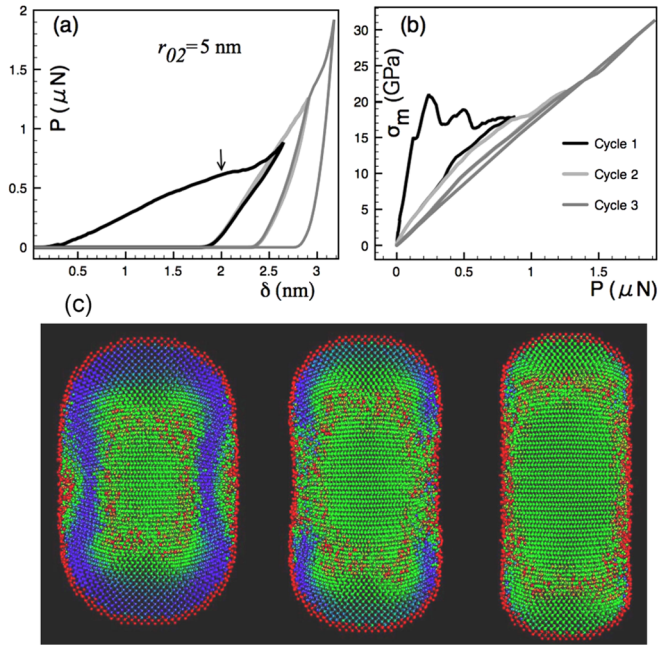

FIG. 4 (color online). (a) Load versus displacement and (b) contact stress versus load. (c) Cross section through the 5 nm particle at the end of each compression cycle.

The β-tin phase has a smaller atomic volume (15 Å^3) than the cubic diamond (20 Å^3), which explains the noted decrease of the particle size. Based on this volumetric difference we can estimate the fraction of atoms in the new phase χ as $v_p[\text{Å}] = 20(1-\chi) + 15\chi$, where v_p is the atomic volume in the compressed particle. For the three configurations shown in Fig. 4(c) we obtained χ values of 30%, 42%, and 58%, respectively.

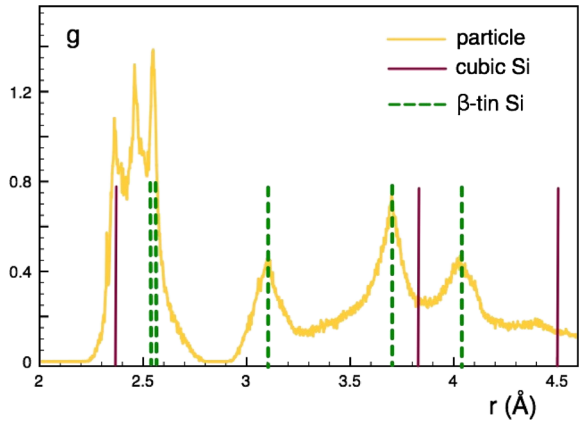

FIG. 5 (color online). Radial distribution function for the 5 nm particle at the end of the third loading cycle. Vertical bars mark the neighbor position in cubic and β-tin Si.

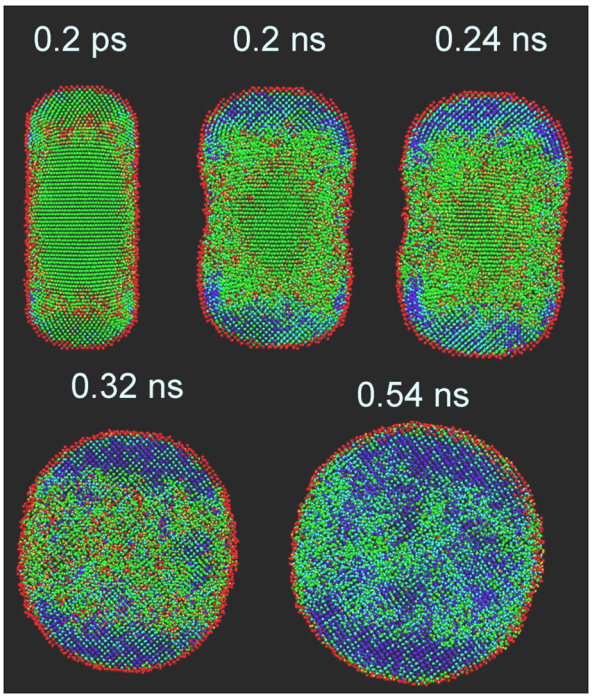

FIG. 6 (color online). Molecular dynamics showing reverse transformation of the highly compressed 5 nm particle.

The higher Young's modulus of the β-tin phase [14] explains the slope increase in the P-δ curves of Fig. 4(a) as well as the hardening effect of Fig. 4(b). For more insight we have created a 5 nm β-tin spherical particle and, following the same compression protocol, we measured a Young's modulus $E_\beta = 550$ GPa, which is indeed significantly higher than the values entered in Table I. It follows that the modulus of the composite cubic-β-tin particle E_p should be larger than that of the original particle E_p^0. For example, we found that for particles with small β-tin content the modulus can be predicted with $1/E_p = (1 - \chi)/E_p^0 + \chi/E_\beta$. For the first configuration of Fig. 4(c) we obtained 134 GPa, in agreement with the value extracted from the unloading curve.

The experimental unloading of severely compressed nanoparticles showed partial reversed plasticity [5]. This observation motivated us to perform constant 1000 K temperature MD simulations on the unstrained metastable structures shown in Fig. 4(c). The velocity Verlet time integration algorithm was used with a time step of 2 fs. Starting from of the most compressed state, the evolution of the 5 nm particle is highlighted in Fig. 6. The size of the β-tin domain decreases with time and the particle gradually looses its barrel-shape. After 0.3 ns the β-tin core undergoes a full reverse transformation to the tetrahedral configuration and the particle snaps into a spherical shape, almost identical with the original one. Experimentally, when particles beyond 20 nm were severely compressed and then released, a residual strain of $\sim$17% was measured, such that nearly half was not recovered. This suggests that a dislocation plasticity mechanism emerges between these two size limits.

To describe the hydrostatic pressurization of 5 to 20 nm in radius Si crystallite [6], a simultaneous coherent transformation model to the β-tin phase was previously proposed [15]. Because in the uniaxial Hertzian compression a nonuniform strain distribution is created in the particle (see the TEM images of Ref. [16]), the coherent model is less valid. We presented here a model in which the nucleation β-tin phase occurs in the particle core at the maximal strain concentration and rapidly propagates in the high-strain regions. The resulting volumetric changes, increase in elastic moduli, and hardening, as well as the reverse transition are all in agreement with experimentation at a slightly different length scale [5]. Thus, phase-transition plasticity appears as an important mechanism even in the compression of 20 to 100 nm in radius Si particles.

Supported by NSF-NIRT CTS-0506748 and NSF CMS 0322436. Calculations performed at the Minnesota Supercomputing Institute.

*Corresponding author.
td@me.umn.edu.

[1] H. G. Craighead, Science **290**, 1532 (2000).
[2] A. M. Minor *et al.*, Philos. Mag. **85**, 323 (2005).
[3] M. I. McMahon and R. J. Nelmes, Phys. Rev. B **47**, 8337 (1993).
[4] V. Domnich, Y. Gogotsi, and S. Dub, Appl. Phys. Lett. **76**, 2214 (2000).
[5] W. W. Gerberich *et al.*, J. Mech. Phys. Solids **51**, 979 (2003); W. W. Gerberich *et al.*, Int. J. Plast. **21**, 2391 (2005); W. M. Mook *et al.*, Phys. Rev. B **75**, 214112 (2007).
[6] S. H. Tolbert *et al.*, Phys. Rev. Lett. **76**, 4384 (1996).
[7] P. Valentini and T. Dumitrică, Phys. Rev. B **75**, 224106 (2007).
[8] J. Tersoff, Phys. Rev. B **37**, 6991 (1988).
[9] R. Rurali and E. Hernandez, Comput. Mater. Sci. **28**, 85 (2003).
[10] R. Martonaka *et al.*, J. Chem. Phys. **117**, 11 329 (2002).
[11] M. Cococcioni *et al.*, Phys. Rev. Lett. **94**, 145501 (2005).
[12] K. Johnson, *Contact Mechanics* (Cambridge University Press, Cambridge, England, 1985).
[13] S. G. Manyes *et al.*, J. Chem. Phys. **123**, 114711 (2005).
[14] The Tersoff potential overestimates the [100] Young's modulus for β-tin Si. A value of 263.26 GPa was obtained with DFT within the local density approximation and the Ceperley-Alder exchange and correlation, G. Kresse *et al.*, http://cms.mpi.univie.ac.at/VASP. As this is significantly higher than in cubic Si, the emerging β-tin domain will still lead to hardening.
[15] L. E. Brus, J. A. W. Harkless, and F. H. Stillinger, J. Am. Chem. Soc. **118**, 4834 (1996).
[16] J. Deneen *et al.*, J. Mater. Sci. **41**, 4477 (2006).